Supplemental Material

"Phase diagram of the $(Pr_{1-y}Sm_y)_{0.7}Ca_{0.3}CoO_3$ system: valence and spin state transition versus ferromagnetism"

Y. Bréard, F. Veillon, L. Hervé, and V. Hardy
Normandie Univ, ENSICAEN, UNICAEN, CNRS, CRISMAT, 14000 Caen, France.

F. Guillou
Inner Mongolia Key Laboratory for Physics and Chemistry of Functional Materials, Inner Mongolia Normal University, 81 Zhaowuda Road, Hohhot 010022, Inner Mongolia, People's Republic of China

K. Kummer, F. Wilhelm, and A. Rogalev
ESRF European Synchrotron, 71 Avenue des Martyrs, F-38000 Grenoble, France

R.I. Smith
Rutherford Appleton Lab, ISIS Pulsed Neutron & Muon Source, Harwell Campus, Didcot OX11 0QX, Oxon, England

---

This Supplementary section addresses the following issues :

1/ Signature of T_C on the *C(T)* curves

2/ Shape of the *M(B)* curves at low *T*

3/ Temperature dependence of the magnetoresistance

4/ Training and hysteretical effects at the VSST

5/ Phase diagram and resistivity

6/ Criteria used to derive T_C, T^* and T_{SRO}

7/ Co spin state at RT from XAS

8/ Magnetic investigation of the system $Pr_{1-x}Ca_xCoO_3$ ($0 \leq x \leq 0.4$)

9/ Absence of signature of SRO around RT in $Pr_{0.7}Ca_{0.3}CoO_3$

10/ T_C versus $\langle r_A \rangle$ in $RE_{0.7}AE_{0.3}CoO_3$ perovskites

11/ Curie-Weiss response of Co around RT in $Pr_{0.7}Ca_{0.3}CoO_3$

12/ Co magnetism from XMCD

13/ Magnetoresistance in $Pr_{0.7}Ca_{0.3}CoO_3$

14/ Structural parameters of $(Pr_{1-y}Sm_y)_{0.7}Ca_{0.3}CoO_3$ derived from tofPND

1/ Signature of T_C on the *C(T)* curves

The heat capacity curves of $(Pr_{1-y}Sm_y)_{0.7}Ca_{0.3}CoO_3$ compounds in the ferromagnetic regime ($y < 0.175$) do not show a clear peak at the T_C. However, the comparison between $y = 0$ and $y = 0.15$ suggests the possibility of a broad feature centered around its T_C for $y = 0$. The reasons allowing such a feature are the following: First, these two compositions do not undergo VSST and they should have very similar lattice contribution (which is the dominant contribution in both cases within the T range of interest); Second, the ferromagnetism (and the T_C) are sizeably weaker (smaller) in $y = 0.15$ than in $y = 0$. As a result, the difference between the *C(T)* curves of these two compositions can yield a fairly precise picture of the magnetic contribution present in $y = 0$. It is found that the difference [*C(T,y=0)-C(T,y=0.15)*] exhibits a broad and weak hump centered around ~ 50 K, which is the temperature corresponding to the midpoint transition in magnetization for $y = 0$.

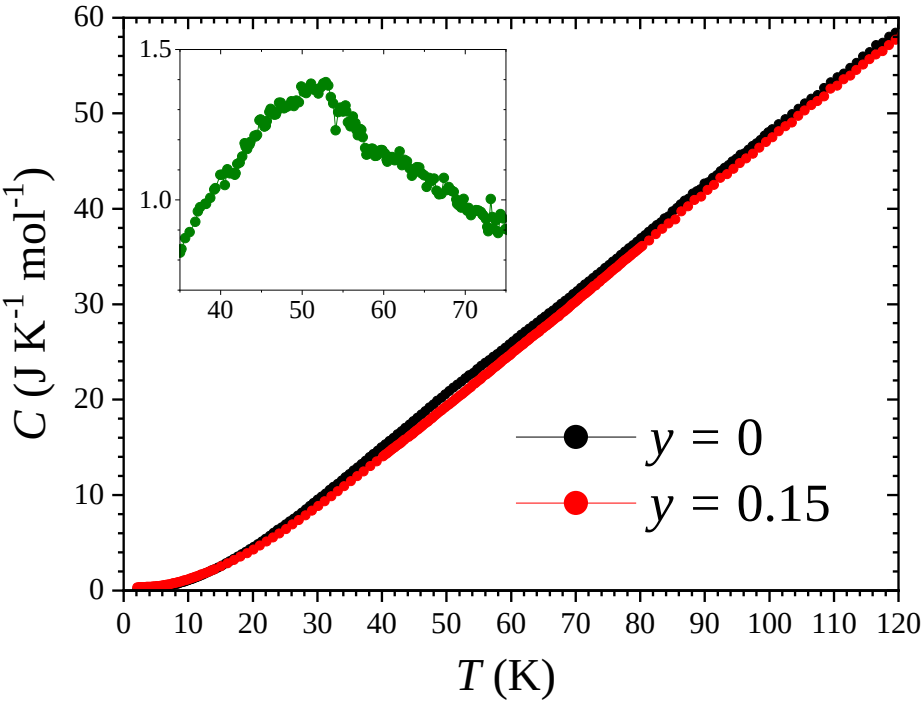

Fig SM1: Heat capacity curves for the y values marking the boundaries of the ferromagnetic regime. The inset displays the difference [*C(T,y=0)-C(T,y=0.15)*].

2/ Shape of the *M(B)* curves at low *T*

Figure SM2 complements the *M(B)* data of Fig. 5(a) in the manuscript, by showing the hysteresis (or not) and the field dependence up to 14 T, for two values of y at the opposite

boundaries of the explored *y*-range in $(Pr_{1-y}Sm_y)_{0.7}Ca_{0.3}CoO_3$. The ferromagnetic regime (y = 0) has a "hard" response (remanence and coercive field), while the shape of the curve for a VSST compound (y = 0.36) evokes that of a "soft" ferromagnet (supporting the presence of a ferromagnetic component below T^*, even though it is weak). In both cases, the magnetization shows a rounded increase, but it does not saturate even in fields as high as 14 T.

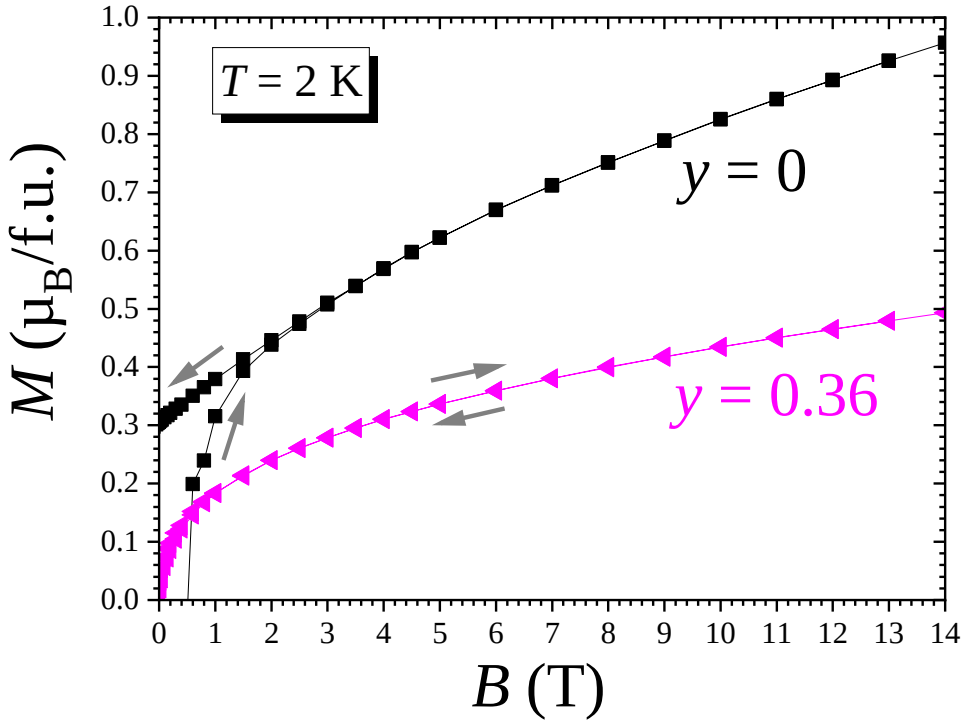

Fig SM2: Magnetic hysteresis curves (first quadrant) recorded at 2 K, in fields up to 14 T (PPMS, Quantum Design), for two *y* values: y = 0, representative of the ferromagnetic regime, and y = 0.36, representative of the VSST regime. The arrows indicate the direction of the field variation.

3/ Temperature dependence of the magnetoresistance

Figure SM3 displays the *MR* ($= [\rho(B) - \rho(0)]/\rho(0)$) derived from $\rho(B)$ curves at various temperatures up to 140 K. It complements the data shown in the manuscript [Fig. 5(b)], which focused on the low-T regime. The major features in Fig. SM3 are the signatures of T_C (negative bumps) and of T^* (negative peaks). Note that the latter tends to weaken as y is increased, as expected for a transition becoming more and more diffuse.

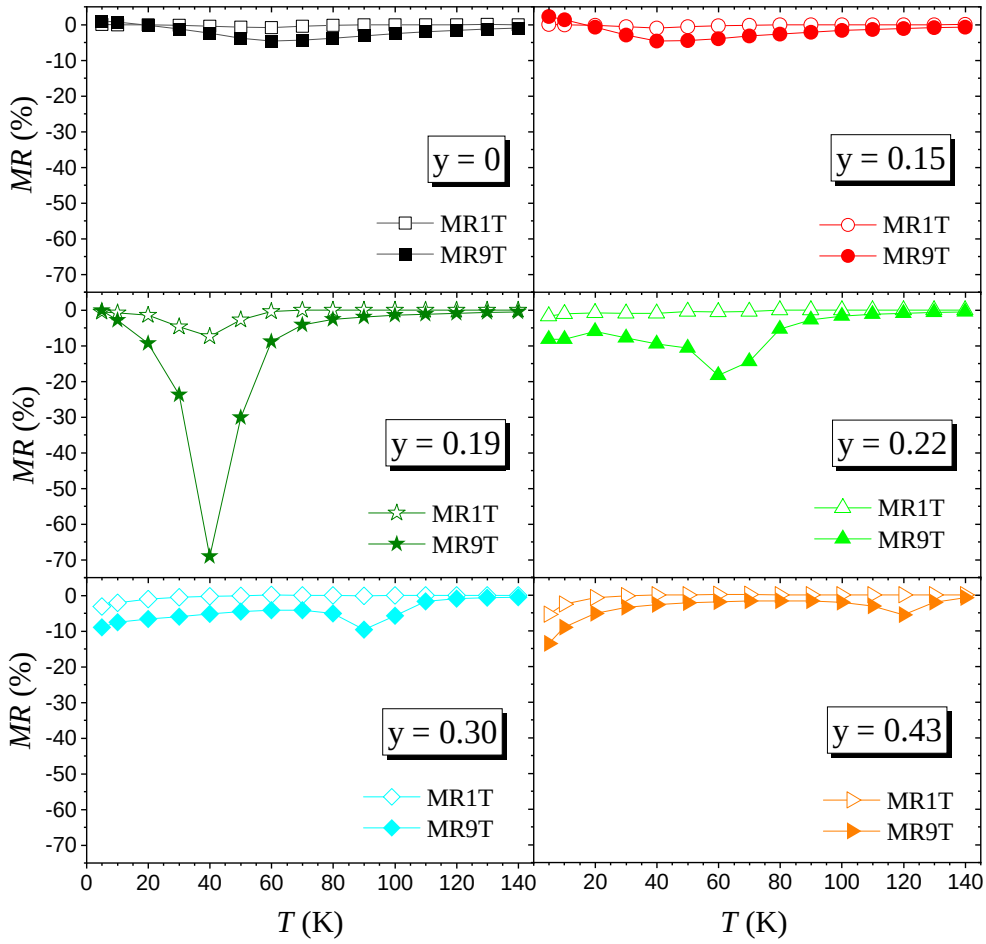

Fig SM3: Temperature dependence of the magnetoresistivity for selected *y* values. These data are derived from *MR(B)* curves recorded a fixed temperatures; they are plotted here for two values of *B* (1 and 9 T). For the sake of comparison, the same scales are used for all *y* values.

4/ Training and hysteretical effects at the VSST

Care should be taken when deriving the characteristic temperature of the VSST (*T**), owing to some features typical of first-order magnetostructural transitions. It turns out that the $(Pr_{1-y}Sm_y)_{0.7}Ca_{0.3}CoO_3$ compounds exhibit some of these features. First, they can be subject to a training effect, i.e. some undercooling along the first crossing of the transition (see Fig. SM4a). Second, an hysteresis –albeit small- can be discerned in the magnetic data (see Fig. SM4b).

Accordingly, we systematically discarded the first cooling and –except for the spontaneous magnetization- we considered magnetization curves recorded in the field-cooled warming mode at a sweep rate of 0.5 K /min.

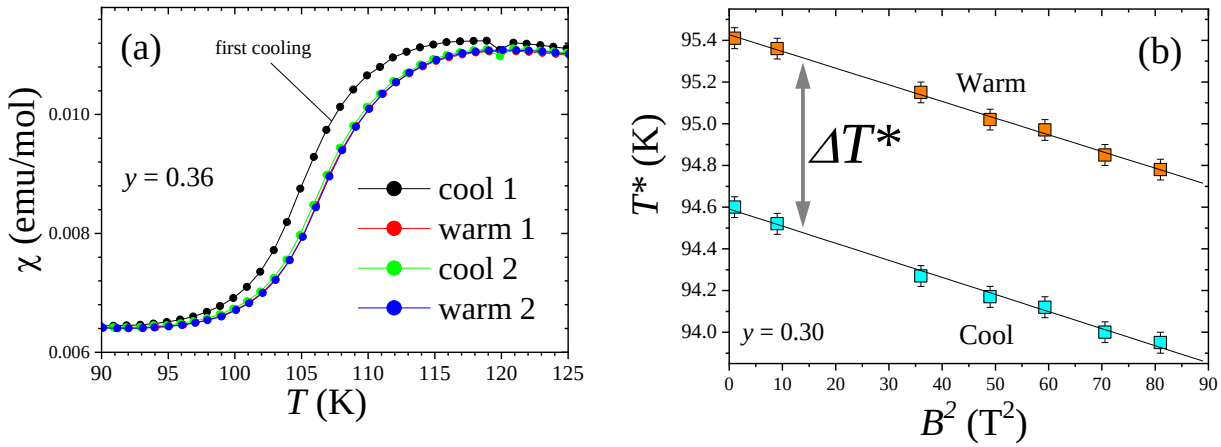

Fig SM4: (a) Illustration of the training effect in the case of $y = 0.36$, showing the susceptibility curves recorded along four consecutive temperature sweeps across T^*. The curve "cool 1" corresponds to the first cooling of the sample below room temperature. (b) Field dependence and hysteresis of T^*, derived from magnetization curves recorded in various magnetic fields, either upon warming or cooling (case of $y = 0.30$).

5/ Phase diagram and resistivity

The resistivity data were not used to build the phase diagram, but they are consistent with it, as shown below.

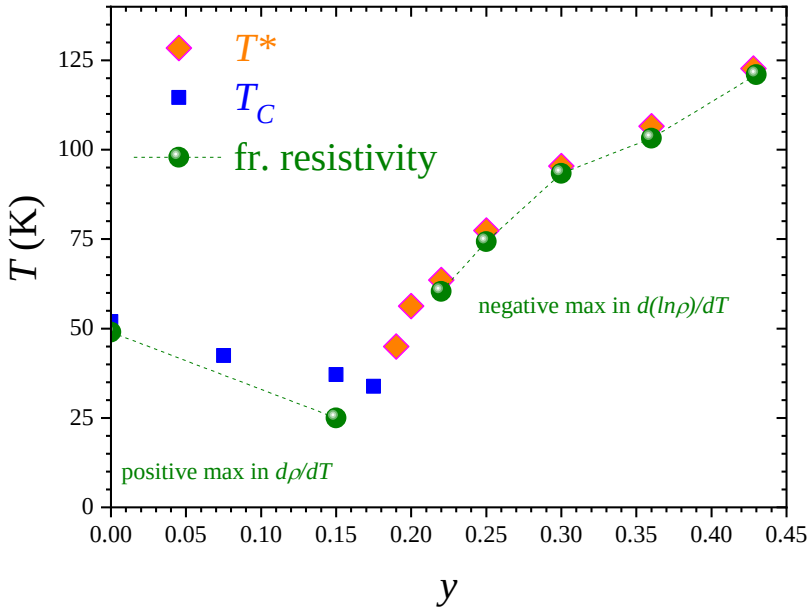

Fig SM5: Incorporation of data derived from resistivity in the phase diagram. In the FM regime, we considered the position of the inflection point below the hump. In the VSST regime, we considered the inflection point of the huge increase in resistivity below T^*. In the latter case, the concordance in temperature with the signatures on the other physical properties is very good. In the FM regime, the features in resistivity are weaker (increasingly so as y increases), and the agreement with magnetism is only semi-quantitative

6/ Criteria used to derive T_C, T^* and T_{SRO}

These characteristic temperatures (reported in the phase diagram of Fig. 6 in the manuscript) have been derived from the spontaneous magnetization curves (cooling in a field of about 1.5 Oe), by following the analysis described in the caption of Fig. SM6.

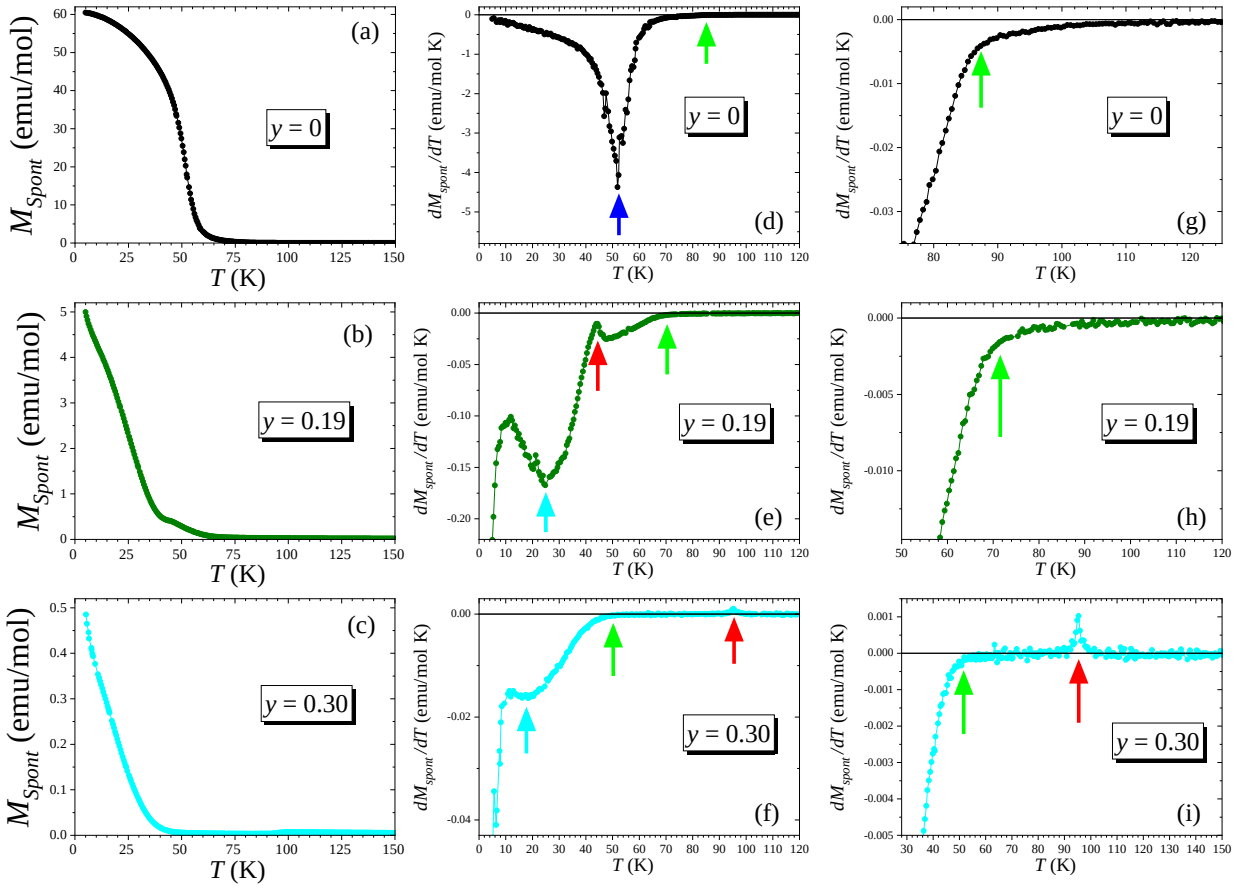

Figure SM6: Illustrations of the plots used to locate the characteristic temperatures. Three y values spanning the investigated range are considered (from top to bottom): y = 0 (FM regime), y = 0.19 (close to y_{crit}), and y = 0.30 (VSST regime). The left panels display the spontaneous magnetization, while the two other columns of panels show the derivative dM_{spont}/dT. Minima in dM_{spont}/dT mark a FM-like ordering; it is either an absolute minimum –in the ferromagnetic regime (blue arrow) – or a local minimum when VSST takes place (cyan arrow). The VSST at T^* corresponds to a maximum (red arrow). It is absent for y = 0. The most uncertain temperature is that marking the beginning of ferromagnetic ordering within clusters (T_{SRO}); however, a characteristic temperature can be derived from the rise of a clear kink in dM_{spont}/dT (green arrow); enlargements around these kinks attributed to T_{SRO} are shown in the right panels.

7/ Co spin state at RT from XAS

XAS experiments were conducted at the Co-*K* and $L_{2,3}$ edges, at low-*T* (5 K) and at room temperature (RT ~ 295 K >> *T**), with the aim of characterizing the Co^{3+} spin state. First, we note that the most noticeable changes occurring at the Co *K* edge when crossing VSST are located in the pre-peak around 7712 eV (see the case of y = 0.36 in Fig. SM7). While the quadrupolar or dipolar origin of the pre-peak remains a debated issue in cobalt oxides, there is an overall consensus that spectral changes in the pre-edge reflect a transition from Co^{3+} LS toward a higher spin-state (see [52] and references therein). Assuming that the double peak structure of the pre-peak in y = 0.36 at 5 K mainly reflects transitions into t_{2g} (~7712 eV) and e_g (~ 7714.2 eV) orbitals, the weakening of the e_g spectral feature when crossing the VSST upon heating can be ascribed to Co^{3+} LS transiting to a higher spin state.

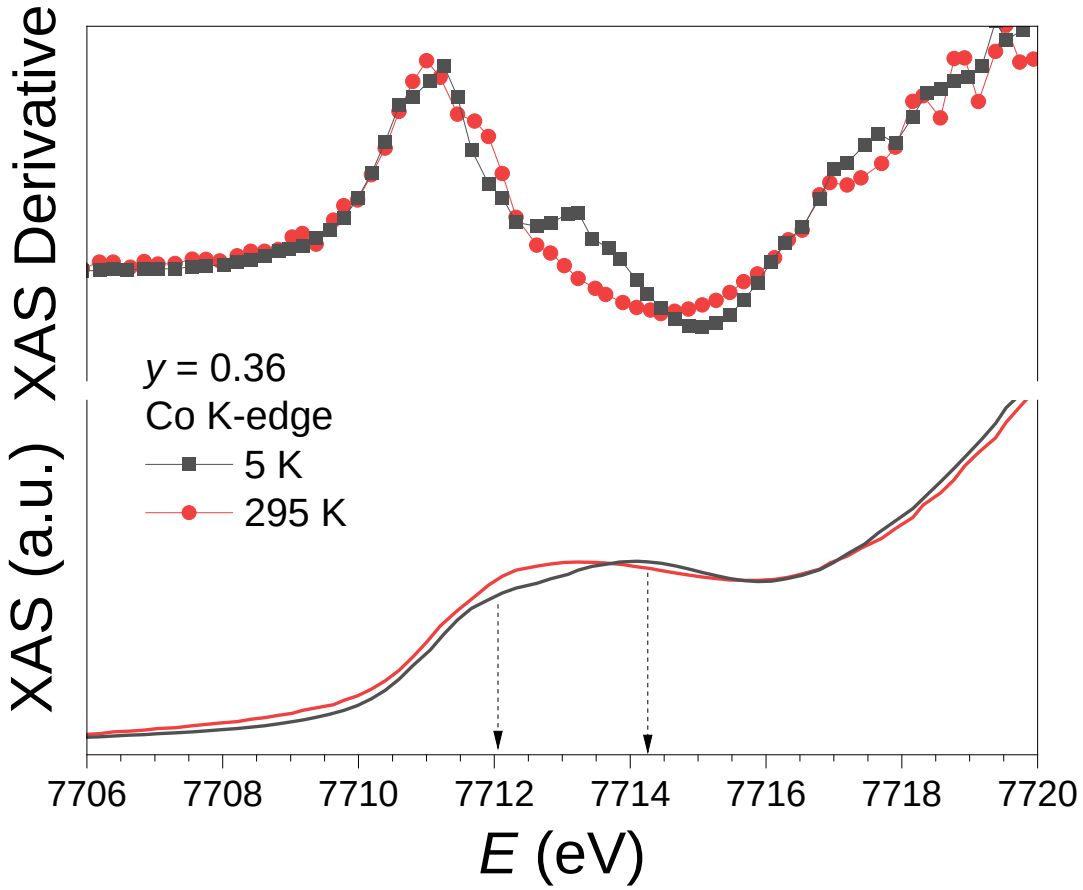

Figure SM7 : XAS spectra at the Co-*K* edge for y = 0.36 across the VSST: enlargement of the pre-peak region. An evolution of the double peak structure is clearly distinguishable at 5 K, both in the raw XAS spectra and in their derivative.

In stark contrast, no such pre-edge evolution could be distinguished at RT as a function of *y*. Figure SM8 presents Co-*K* edge measurements at RT for the full *y* range. With the exception

of the y = 0.5 sample showing a slight increase in intensity in the rising part of the edge around 7222 eV (mostly likely originating from minor Co^{2+} contamination), no significant spectral changes could be observed, giving a first indication of nearly identical Co spin-state at RT along the y series.

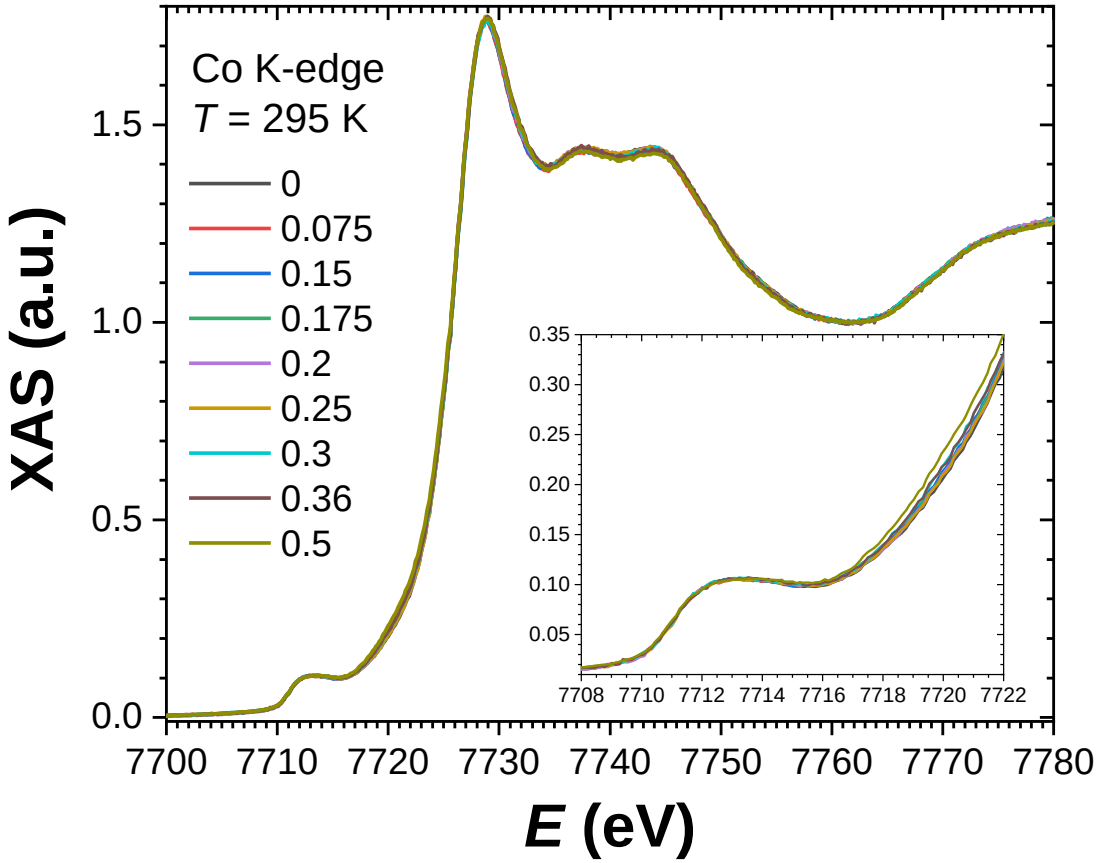

Figure SM8 : Co-*K* edge XAS spectra of $(Pr_{1-y}Sm_y)_{0.7}Ca_{0.3}CoO_3$ samples recorded at room temperature for nine y values. The nearly perfect superimposition of these curves indicate that the valence and spin state of cobalt –in this high-T range– is almost the same for all y values.

In addition, XAS experiments at RT were carried out at the Co-$L_{2,3}$ edges in $(Pr_{1-y}Sm_y)_{0.7}Ca_{0.3}CoO_3$ for three y values: 0, 0.3, and 0.36 (see Fig. SM9). The spectral differences between these three samples remain very subtle, in line with the Co-*K* edge results. One can just note a slightly higher intensity in the shoulder around 780 eV for y = 0 which might be indicative of higher Co^{3+} HS content, while the sharper peak at 796.5 eV for y = 0.36 could be ascribed to higher Co^{3+} LS content. Using the analysis described in [18], these spectra were fitted by considering 30% of Co^{4+} LS and 70% of Co^{3+} showing a mixture LS/HS. Within such a framework, the results lead to a Co^{3+} HS/ Co percentage —at RT— of approximately 42%, 37% and 34%, for y = 0, 0.3 and 0.36, respectively.

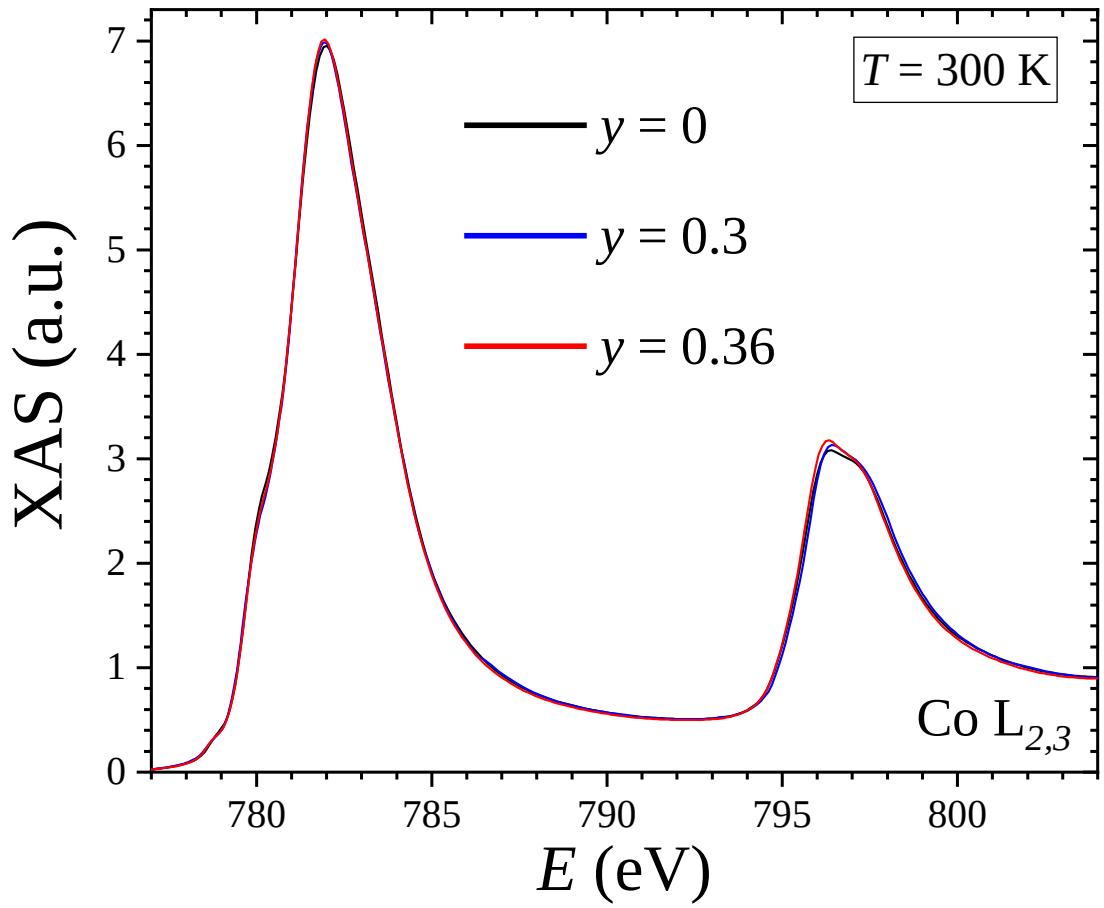

Figure SM9 : Enlargement of XAS spectra at the Co-*L* edges, recorded at RT for three *y* values. The almost total superimposition of these curves indicate that the valence and spin state of cobalt –in this high-*T* range– is almost the same for all *y* values.

8/ Magnetic investigation of the system $Pr_{1-x}Ca_xCoO_3$ ($0 \leq x \leq 0.4$)

Magnetic susceptibility curves of $Pr_{1-x}Ca_xCoO_3$ compounds were recorded in a field of 0.1 T (FCW mode) for eight *x* values in the range 0 - 0.4. These curves are shown in Fig. SM10(a) using a semi-log scale owing to the huge variation in the susceptibility as a function of *x*.

The lower panels illustrate (for the lowest and highest *x* values) the effect of the subtraction of the Pr^{3+} magnetism estimated by Tsubouchi *et al.* in related cobaltates [35]. Within the low-*x* side, this reveals the signature of the SST, while it has very marginal effect as soon as the ferromagnetic response emerges.

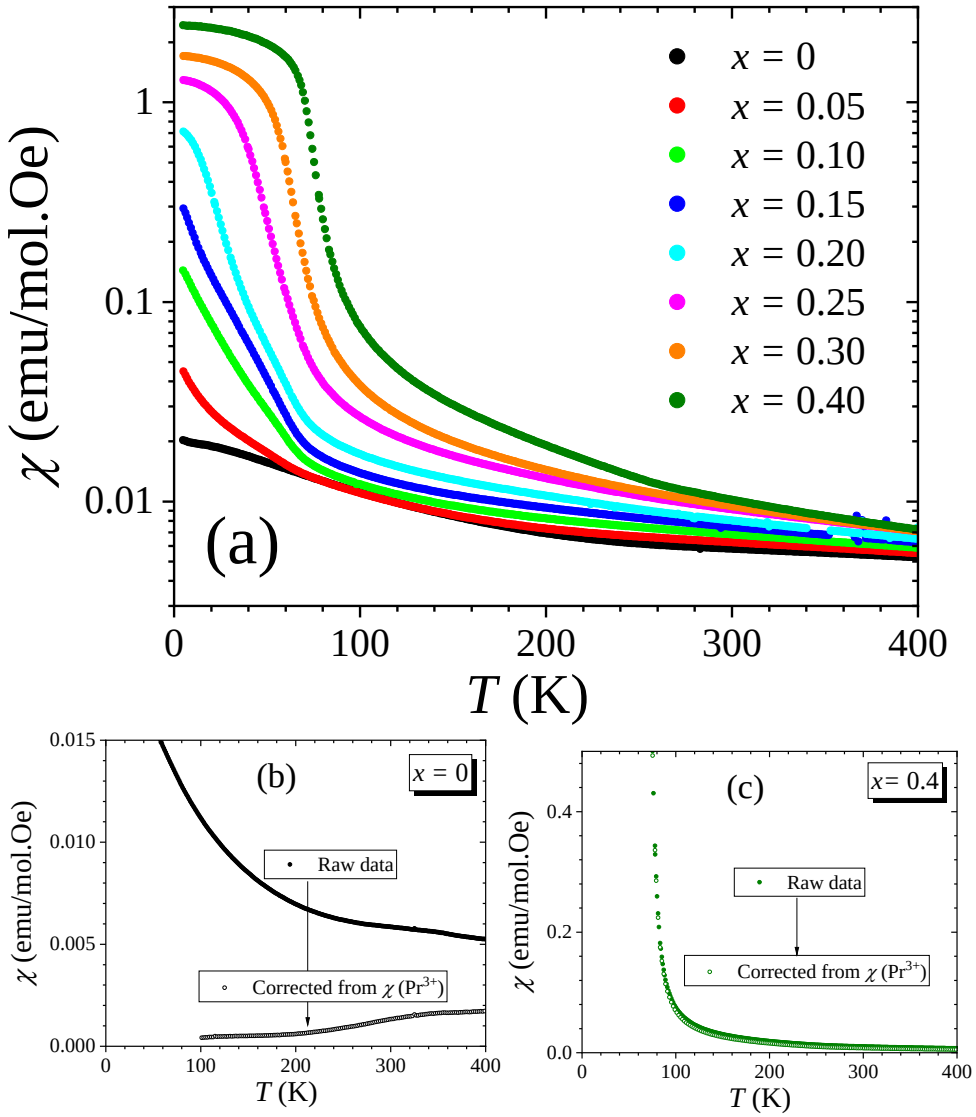

Figure SM10: (a) Susceptibility curves for various x values within the $Pr_{1-x}Ca_xCoO_3$ system; (a) Susceptibility curves of $x = 0$ before and after the subtraction of the Pr^{3+} contribution; (c) Same data for $x = 0.4$. Note that the Tsubouchi's approximation was originally derived for $T > 100$ K (reason why the Pr^{3+} correction is limited to this range in (a) where the competing low Co-magnetism is small).

9/ Absence of signature of SRO around RT in $Pr_{0.7}Ca_{0.3}CoO_3$

In their study of $Pr_{0.7}Ca_{0.3}CoO_3$, El Khatib *et al.* reported a marked anomaly on the susceptibility curve around 250 K, that was ascribed to the emergence of ferromagnetic clusters (SRO) [36]. This anomaly takes the form of a sudden step on the FCC curve at ~ 250 K (see Fig. 2 of [36]).

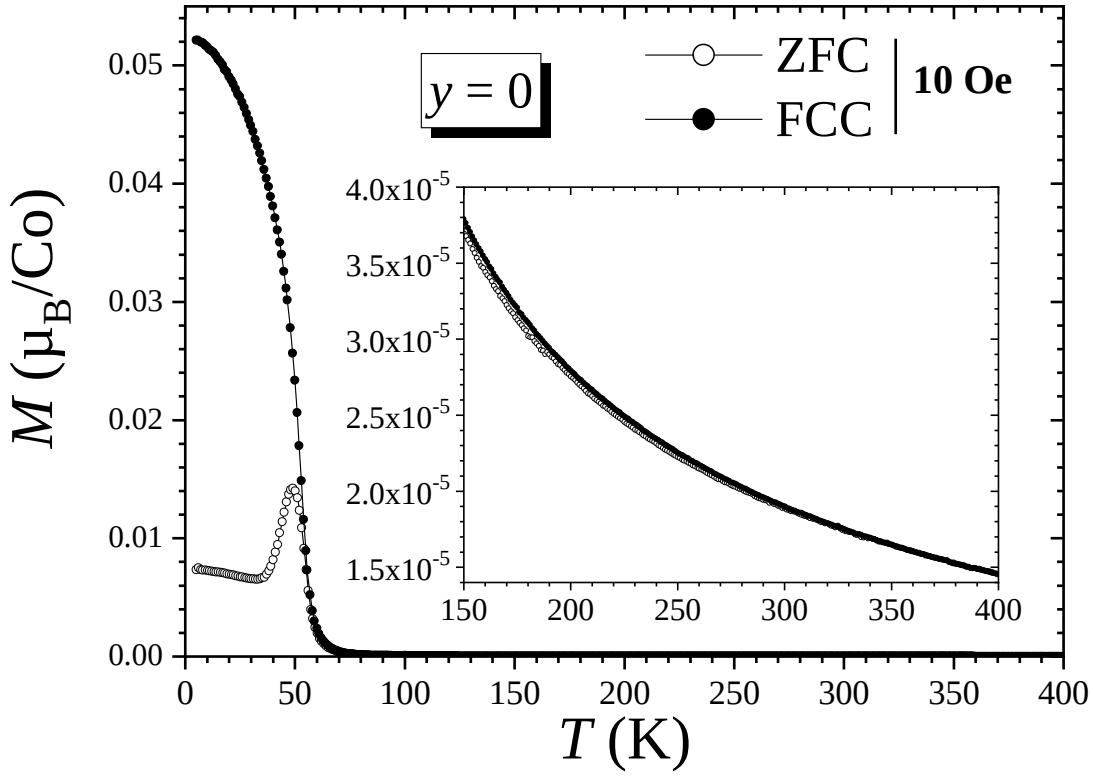

Fig SM11: Magnetization curves of $Pr_{0.7}Ca_{0.3}CoO_3$ recorded in a low field of 10 Oe, using Zero-Field-Cooled and Field-Cooled-Cooling modes. The inset is an enlargement around room temperature.

In Fig. SM11, we show our data measured in the same conditions and presented in the same units. It is clear that no anomaly similar to that of Ref. [36] is present. If we take a very close look, one may just consider that the divergence between ZFC and FCC branches starts progressively from ~ 300 K. Knizek *et al.* also reported the absence of the "250 K feature" in their materials [27]. Since it was suggested that this anomaly might be connected to oxygen deficiency [30,36], it is quite possible that small differences in synthesis procedures (which could be expected to affect the oxygen stoichiometry) can play a role in the existence or not of such an anomaly around RT. This also means that this feature should not be regarded as an intrinsic feature of $Pr_{0.7}Ca_{0.3}CoO_3$.

10/ T_C versus $\langle r_A \rangle$ in $RE_{0.7}AE_{0.3}CoO_3$ perovskites

We have collected from the literature values of T_C (derived from susceptibility curves) for different compounds obeying the general formula $RE_{0.7}AE_{0.3}CoO_3$, where RE is a (trivalent) rare-earth and AE a (divalent) alkaline-earth.

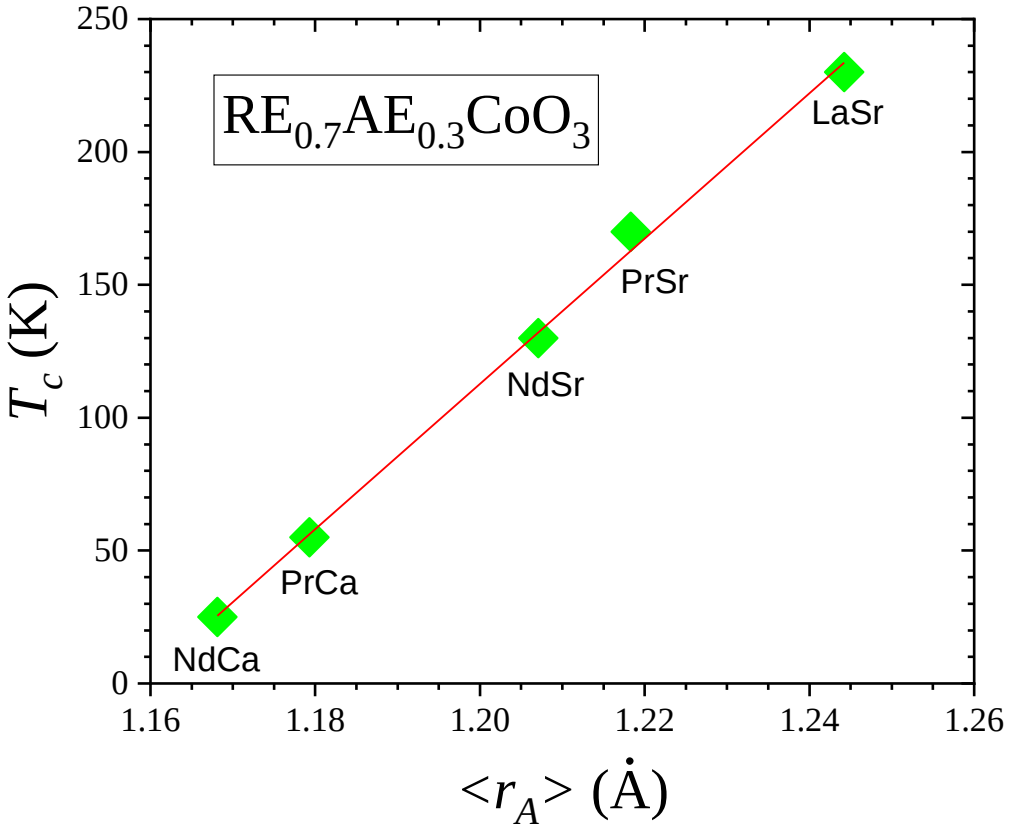

Fig SM12: Values of Curie temperature in perovskite compounds of formula $RE_{0.7}AE_{0.3}CoO_3$, where RE is a (trivalent) rare-earth and AE a (divalent) alkaline-earth. These T_c are derived from the inflection point on the susceptibility curve (low field). Our plot aggregates data taken from two papers of the literature: [28] for $Nd_{0.7}Ca_{0.3}CoO_3$, $Pr_{0.7}Ca_{0.3}CoO_3$, $Nd_{0.7}Sr_{0.3}CoO_3$, and $La_{0.7}Sr_{0.3}CoO_3$, and [46] for $Pr_{0.7}Sr_{0.3}CoO_3$.

The average cationic radius on the A sites is calculated by the formula: $\langle r_A \rangle = 0.7\, r_{RE^{3+}} + 0.3 r_{AE^{2+}}$, considering values of cationic radii in ninefold coordination (Shannon-Prewitt tables). The red line is a linear fitting which reasonably reflects the T_C variation versus $<r_A>$: $T_C(K) = -3168 + 2733\, \langle r_A \rangle$ (Å)

11/ Curie-Weiss response of Co around RT in $Pr_{0.7}Ca_{0.3}CoO_3$

Figure 2 of the manuscript displays the "raw" $1/\chi(T)$ around RT. To isolate the Co response several contributions must be removed, the most prominent being that coming from the rare earths (Pr and Sm). Here, we detail the procedure used for the whole series, by focusing on the best known composition $y = 0$.

The Curie-Weiss contribution associated with the Co (denoted χ^{Co}) has been derived as follows: First, the Pr^{3+} contribution has been subtracted from the raw data by using the

Tsubouchi's approximation: χ^{Pr3+}(emu/mol)=1.6/[T(K)+54] [35]. Then, the diamagnetic component χ_{dia} (= -0.63 10^{-4} emu/mol) was removed too, as well as an additional Temperature-Independent-Paramagnetic (TIP) term denoted $\chi_{0.}$ This latter component should incorporate a contribution coming from the van Vleck TIP of Co^{3+} LS, as well as a Pauli term related to that of $LaCoO_3$, since our compounds exhibits the same type of metallic-like conductivity around RT. In $LaCoO_3$, Jirak *et al.* suggested a χ_{Pauli} of the order of 4 10^{-4} emu/mol [50]. Since the average spin state of Co^{3+} is approximately the same in the present y = 0 compound (i.e., Co^{3+} HS / Co^{3+} LS ~ 1) a Pauli term of similar value can be reasonably anticipated. As for χ_{vv}(Co^{3+} LS), it is reported to be about 2 10^{-4} emu/mol [51]. It is a fact that there is a significant uncertainty about the value of χ_0. We decided to use a χ_0 value yielding a paramagnetic moment consistent with the cobalt spin state derived from XAS studies. This led us to set χ_0 = + 5 10^{-4} emu/mol, a value well compatible with the estimates of χ_{VV} and χ_{Pauli} discussed above.

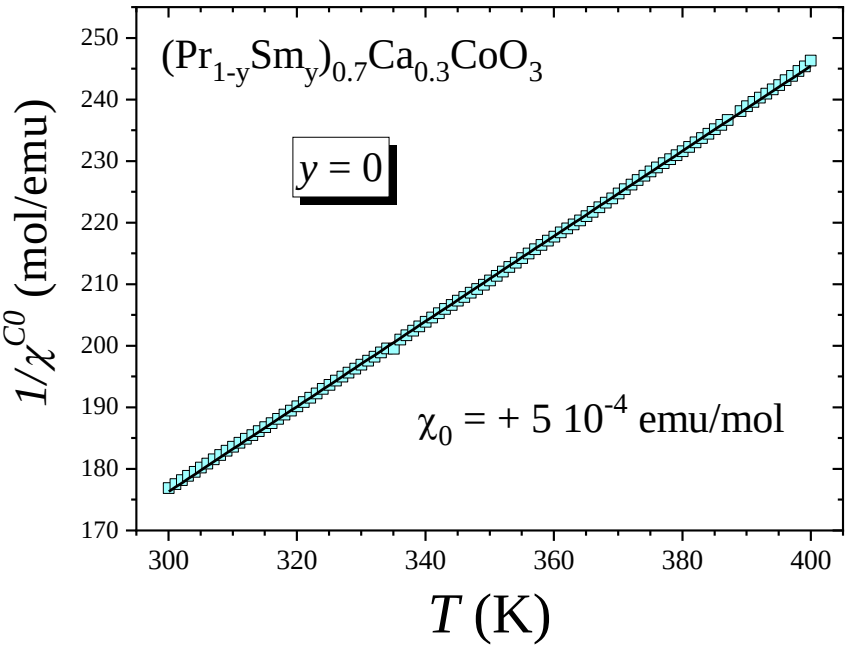

Fig SM13: Reciprocal susceptibility of Co in $Pr_{0.7}Ca_{0.3}CoO_3$ when setting a χ_0 equal to 5 10^{-4} emu/mol. The squares are the data limited to the range 300-400 K over which a linear fitting was performed (black line).

The reciprocal susceptibility of cobalt obtained from $\chi^{Co} = \chi_{raw} - \chi(Pr^{3+}) - \chi_{dia} - \chi_0$ is shown in Fig. SM13. A Curie-Weiss fitting within the 300-400 K range leads to μ_{eff} (Co)=3.4 μ_B. Such a value is inconsistent with a magnetism stemming only from Co^{4+}, indicating that at

least a part of the Co^{3+} is in a spin state higher than LS. We will consider that a fraction *f* of Co^{3+} are in a HS state. This fraction is given experimentally by $f = \{(\mu_{eff})^2 - 0.3\ [\mu_{eff}(Co^{4+})]^2\}$ / $\{0.7\ [\mu_{eff}(Co^{3+}HS)]^2\}$. Adopting usual approximations of the effective moments $\mu_{eff}(Co^{4+}$ LS) = 1.73 μ_B and $\mu_{eff}(Co^{3+}$ HS) = 4.90 μ_B (around RT), one obtains $f = 0.63$. This means that — in $Pr_{0.7}Ca_{0.3}CoO_3$ at RT —the percentage of cobalt cations being Co^{3+} HS is 44% (= 63*0.7). This value is well consistent with that derived from XAS experiments (42% from Fig. SM9), which thereby justifies the adopted value of χ_0. Figure SM13 shows that the susceptibility of Co exhibits a Curie-Weiss regime from which a Curie-Weiss temperature *reflecting the effective interactions within the Co sublattice* can be extracted. It yields $\theta_{CW} \sim$ 45 K for $y = 0$.

Let us add two remarks: (i) Having a mixed Co^{3+} spin state for $Pr_{0.7}Ca_{0.3}CoO_3$ around RT is consistent with the position of the Spin State Transition line reported in Fig. 9(c) of the manuscript; (ii) Having a coexistence of Co^{4+} LS and Co^{3+} HS is consistent with the development of a Double Exchange mechanism at the origin of a ferromagnetic response (even though this FM is diluted by the presence of a substantial part of the Co^{3+} being in a non-magnetic LS state).

12/ Co magnetism from XMCD

The magnetism of $Pr_{0.7}Ca_{0.3}CoO_3$ is tricky and still intensively debated. From an experimental viewpoint, the situation is made complex by the mixing of the Co and Pr contributions to the magnetization measurements. It is the kind of situation for which X-ray Magnetic Circular Dichroism (XMCD) is an ideal probe as it allows the magnetization associated with a given species to be isolated.

In a recent experiment, we have investigated in detail the case of $y = 0.36$ by XMCD (ID 32 beamline at ESRF) [18]. To be used as a reference, the composition $y = 0$ was also measured in this experiment. This data is shown in Fig. SM14.

First, this confirms that the remanence of 0.3 μ_B/fu shown on the hysteresis loop [Fig. 5(a) of the manuscript] is coming from the Co (as expected). More importantly, Fig. SM14(a) demonstrates that the Co magnetization continuously increases as the field is increased. The saturation is not reached up to 9 T, but one can estimate it might be of the order of ~ 0.6 μ_B/Co. This value is important to decorrelate the Co and Pr contributions to the overall magnetization (see discussion in the manuscript).

In addition, XMCD measurements were also performed at RT for different *y* values (see Fig. SM15). The integrals of XMCD curves clearly decrease with increasing *y*. Co moments calculated using the magneto-optical sum-rules (with n_h = 4.3 and neglecting the T_z operator) are 0.10, 0.09, 0.07 and 0.05 μ_B/Co for *y* = 0, 0.2, 0.36 and 0.5, respectively. The decrease in Co magnetization at RT when *y* increases is both qualitatively and quantitatively in line with the reciprocal Co susceptibility derived from bulk magnetic measurements presented in Fig. 10 of the manuscript.

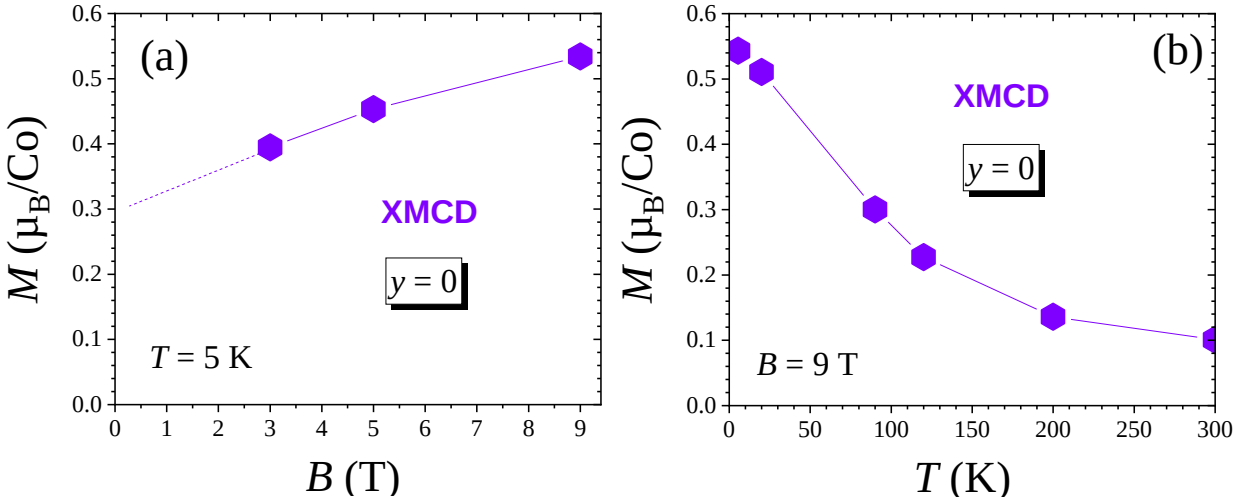

Fig SM14: Magnetization of Co in $Pr_{0.7}Ca_{0.3}CoO_3$ derived from XMCD experiments. Panel (a) shows the results at the lowest temperature (5 K) versus the magnetic field value, while panel (b) shows the data versus temperature for the highest field (9 T). The dashed line in (a) is a rough extrapolation to zero-field, showing that one expects a magnetization of ~ 0.3 μ_B/Co.

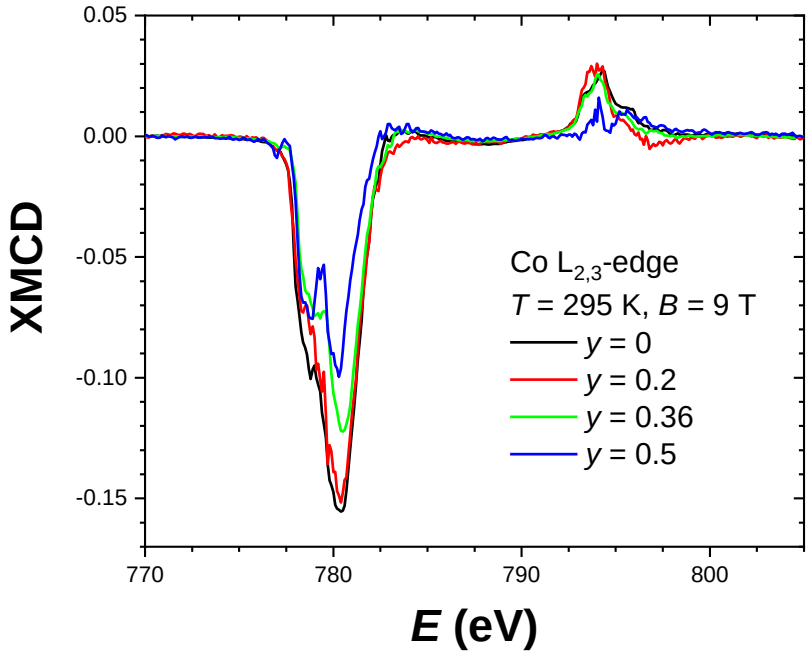

Fig. SM15: XMCD signals at RT and B = 9 T for four $(Pr_{1-y}Sm_y)_{0.7}Ca_{0.3}CoO_3$ samples.

13/ Magnetoresistance in $Pr_{0.7}Ca_{0.3}CoO_3$

The magnetoresistance of the low y compounds at low temperatures is very complex. From Fig.5(b), it was suggested that the *MR* response might be the combination of several antagonistic mechanisms. This hypothesis turns out to be supported by the temperature dependence of the *MR(B)* curves of y = 0 shown in Fig. SM16.

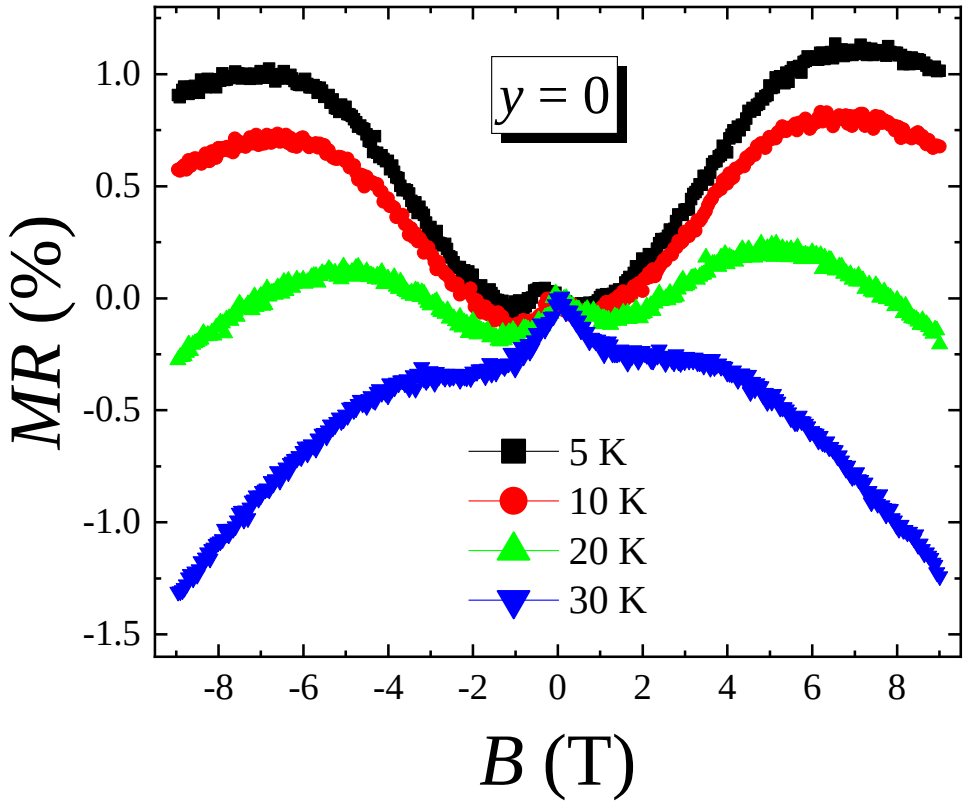

Fig SM16: Field dependence of the magnetoresistivity of $Pr_{0.7}Ca_{0.3}CoO_3$ recorded at several temperatures.

These curves can be described as the combination of at least three mechanisms, whose respective weights vary with the temperature: (i) a positive cusp around zero-field, (ii) a trend towards positive slope at intermediate field, and (iii) an opposite trend to negative slope in higher fields. It is the second mechanism which is at the origin of the positive *MR* at low temperature. As T is increased, the third mechanism develops in lower field and erases the

regime of positive slope. In other respects, we note that the cusp associated with the first mechanism is present at all temperatures.

14/ Structural parameters of $(Pr_{1-y}Sm_y)_{0.7}Ca_{0.3}CoO_3$ derived from tofPND

y		*X*	*Y*	*Z*	*a* (Å)	*b* (Å)	*c* (Å)	θ_1 (°)	θ_2 (°)
0	Pr/Sm/Ca	*0.02978*	*¼*	*-0.00587*	5.3521	7.5704	5.3625	158.299	157.762
	O1	*0.49163*	*¼*	*0.06710*					
	O2	*0.21503*	*-0.03492*	*0.21585*					
0.075	Pr/Sm/Ca	*0.02912*	*¼*	*-0.00585*	5.3503	7.5646	5.3559	157.834	157.498
	O1	*0.49185*	*¼*	*0.06777*					
	O2	*0.21435*	*-0.03566*	*0.21438*					
0.15	Pr/Sm/Ca	*0.03062*	*¼*	*-0.00612*	5.3481	7.5586	5.3504	157.284	157.196
	O1	*0.49171*	*¼*	*0.06981*					
	O2	*0.21359*	*-0.03568*	*0.21333*					
0.25	Pr/Sm/Ca	*0.3064*	*¼*	*-0.00783*	5.3456	7.5517	5.3451	156.867	156.888
	O1	*0.49085*	*¼*	*0.07132*					
	O2	*0.21327*	*-0.03610*	*0.21215*					
0.4	Pr/Sm/Ca	*0.03073*	*¼*	*-0.00543*	5.3426	7.5397	5.3353	155.953	156.435
	O1	*0.49196*	*¼*	*0.07457*					
	O2	*0.21368*	*-0.03671*	*0.21156*					

Table S1 : Structural parameters of $(Pr_{1-y}Sm_y)_{0.7}Ca_{0.3}CoO_3$ at room temperature determined by tofPND. Refinements are performed with the P*nma* Space group. The atomic coordinates of Co are (½,0,0).

References

[18] F. Guillou, K. Kummer, Y. Bréard, L. Hervé, and V. Hardy, Phys. Rev. B 95, 174445 (2017).

[27] K. Knížek, J. Hejtmánek, M. Maryško, P. Novák, E. Šantavá, Z. Jirák, T. Naito, H. Fujishiro, C. de la Cruz, Phys. Rev. B 88, 224412 (2013).

[28] Z. Jirák, J. Hejtmánek, K. Knížek, M. Maryško, P. Novák, E. Šantavá, T. Naito, and H. Fujishiro, J. Phys.: Condens. Matter 25, 216006 (2013).

[30] D. Phelan, K. P. Bhatti, M. Taylor, S. Wang, and C. Leighton, Phys. Rev. B 89, 184427 (2014).

[35] S. Tsubouchi, T. Kyomen, M. Itoh, and M. Oguni, Phys. Rev. B 69, 144406 (2004).

[36] S. El-Khatib, S. Bose, C. He, J. Kuplic, M. Laver, J. A. Borchers, Q. Huang, J. W. Lynn, J. F. Mitchell, and C. Leighton, Phys. Rev. B 82, 100411(R) (2010).

[46] C. Leighton, D. D. Stauffer, Q. Huang, Y. Ren, S. El-Khatib, M. A. Torija, J. Wu, J. W. Lynn, L. Wang, N. A. Frey, H. Srikanth, J. E. Davies, K. Liu, and J. F. Mitchell, Phys. Rev. B 79, 214420 (2009).

[50] Z. Jirák, J. Hejtmánek, K. Knížek and M. Veverka, Phys. Rev. B 78, 014432 (2008).

[51] K. Knížek, Z. Jirák, J. Hejtmánek, M. Veverka, M. Maryško, G. Maris, and T. T. M. Palstra, Eur. Phys. J. B. 47, 213 (2005).

[52] M. Medarde, C. Dallera, M. Grioni, J. Voigt, A. Podlesnyak, E. Pomjakushina, K. Conder, Th. Neisius, O. Tjernberg, and S. N. Barilo, Phys. Rev. B 73, 054424 (2006).